Dimensional analysis and experimental validation for a rotary vane expander operated with air or hydrogen at different feeding pressures

Samuele Beltrametti[1], Francesco Battistella[1], Antonino Ravidà[1], Alessandro Romei[1] and Gianluca Valenti[1]

[1] Politecnico di Milano, Department of Energy, Via R. Lambruschini 4A, 20156, Milan, Italy

Abstract. Rotary vane expanders are employed usually to power tools in industry, using industrial compressed air as working fluid. The commercial rotary vane expanders are designed in accordance with ISO 2787. Because they may be employed also for other scopes, this work evaluates their power and isentropic efficiency when operating with air or hydrogen at different inlet pressures by way of a dimensional analysis, which is carried out considering the variables affecting the performance, such as inlet and outlet pressures and temperatures, gas viscosity, and rotational speed. The outcome of the analysis comprises two dimensionless performance maps: one for power and another for isentropic efficiency. With the use of a specially designed test bench, data for constructing the performance maps are gathered with air and hydrogen. The model is then validated while operating with air or hydrogen under different inlet pressures, ranging from 370 kPa to 720 kPa with expansion ratios between 2.0 and 3.0. The output shows good accuracy in predicting the power and isentropic efficiency of the expander with errors lower than 6.70% and 6.74% respectively.

Keywords: Performance Map, Compressed Gas, Hydrogen, Dynamic Viscosity, Experimental Validation.

1 Introduction

Gases employed in energy conversion systems such as methane, hydrogen, carbon dioxide, argon, and nitrogen are usually stored at high pressure. This implies a high energy expense for compression [1] However, their final use often occurs at a lower pressure than the storage one. Moreover, pressure reduction is usually performed through a valve without recovering any of the energy used for compression. A rotary vane expander can harness part of this energy by reducing the gas pressure while simultaneously driving an electric generator. Rotary vane expanders for single-phase fluids usually power tools in industry and they are designed in accordance with ISO 2787 standards [2]: the working fluid is air, the inlet pressure is 730 kPa and the outlet pressure is approximately the ambient pressure (101.325 kPa). However, the design of such an expander requires the capability of estimating how its performance varies with different inlet and outlet pressures, inlet temperatures, and types of working fluids.

Rotary vane expanders have been extensively studied by Badr *et al.* in a series of works. In particular, they provided models to describe the geometry and kinematics, the losses, and the breathing characteristics [3,4,5]. However, the global description of the behavior of the machine might be performed using dimensional analysis [6]. This analysis is not widely applied to volumetric expanders in the literature. Narashimhan *et al.* and Olmedo *et al.* elaborated two models for the characterization of scroll expanders [7,8]. These models can simulate the performance of the machine through a precise description of the loss mechanisms occurring during operation in different conditions. The results of their simulation provided a series of specific speed-specific diameter (N_s -D_s) diagrams for different fluids and inlet conditions. Francesconi *et al.* studied Wankel expanders with air and steam [9]. They identified their collocation on the Balje Map for the first time and proposed a definition of D_s using the smallest radial dimension of the stator.

This work characterizes a rotary vane expander adopting the dimensional analysis approach. The analysis identifies all the *n* parameters influencing the output power *P* and the isentropic efficiency η_{is}. Using the Buckingham Theorem, the number of variables can be reduced to *n-k* dimensionless parameters, where *k* represents the number of independent dimensions that characterize the system [10]. *k* is also the number of variables of the base used to perform the nondimensionalization. The variables of the base are chosen to be easy to control during experimental tests and to facilitate the identification of dimensionless parameters comparable with those already in literature. Two dimensionless performance maps are built using data collected with air and hydrogen on a specially designed test bench. The maps describe the power and the efficiency of the expander in dimensionless terms. The present study only considers geometrically similar machines and focuses on air and hydrogen as working fluids. The aim of the work is to enable the testing of a rotary vane expander with air and subsequently calculate its performance with hydrogen at higher pressures, simplifying the sizing of a high-pressure hydrogen expander.

2 Dimensional analysis applied to the rotary vane expander

The dimensional analysis is performed first by identifying the variables, the dimensions, and the subsequent base for the derivation of the dimensionless parameters. The set of variables describing the problem can be divided into state variables, fluid properties, geometrical dimensions, and kinematic variables. All the variables and their units are described in the nomenclature section. The variables belonging to each subset are as follows.

- State Variables: inlet temperature T_{in}, inlet pressure p_{in}, and outlet pressure p_{out}.
- Fluid Properties*:* specific heat at constant pressure c_v, gas constant per unit of mass R_g**,**and dynamic viscosity μ.
- Geometrical variables: inlet port diameter D_{in}, internal radius of the machine r_{in}, external radius of the machine r_{ext}, length of the vane L, vane thickness b, inlet port angle θ_{in}, exhaust port opening angle θ_{out}, and number of vanes z.
- Kinematic Variables: rotational speed N.

The power at the shaft and the isentropic efficiency are functions of all the variables listed above and are defined as:

$$P = \dot{m}(h_{in} - h_{out}) \quad (1)$$

$$\eta_{is} = \frac{P}{\dot{m}(h_{in} - h_{out,is})} \quad (2)$$

where h_{in} and h_{out} refer to the inlet enthalpy and outlet enthalpy, and ṁ refers to the mass flow rate processed.

The value of the dynamic viscosity is expected to vary throughout the expansion process since it is highly dependent on the temperature, but its variation is here neglected, as about 60% of all the losses occurring within a rotary vane expander are due to viscous dissipation at the inlet of the machine, as evidenced in literature [5,11]. As a result, the dynamic viscosity is calculated with the inlet conditions. Finally, all the quantities are calculated assuming to deal with an ideal gas as relative pressures are always low for the whole set of gases and operational conditions considered.

The next step of the dimensional analysis involves the derivation of the dimensionless parameters. Indeed, the fundamental dimensions of the problem are four: length, mass, temperature, and time. The four dimensionally independent variables selected as the base are:

- inlet temperature T_{in},
- inlet pressure p_{in},
- gas constant R_g,
- and external radius r_{ext}.

T_{in} and p_{in} are chosen for their ease of control and direct influence on the thermodynamics of the problem. R_g is chosen to represent the variation of the gas thermodynamic properties. r_{ext} is representative of the geometry and it is directly related to the maximum peripheral speed of the machine.

The dimensionless parameters are derived using the matrix-based approach illustrated by Longo [6]. Given the chosen base, the i-th dimensionless parameter is in the form:

$$\Pi_i = \frac{x_i}{T_{in}^{\alpha_i} p_{in}^{\beta_i} R_g^{\gamma_i} r_{ext}^{\delta_i}} \quad (3)$$

where α, β, γ, and δ are rational power coefficients. Furthermore, the isentropic efficiency η_{is}, the number of vanes z, the inlet port angle θ_{in}, and the exhaust port opening angle θ_{out} are already dimensionless and they are left unchanged throughout the nondimensionalization process. The heat capacity ratio and the expansion ratio were derived from two parameters obtained as the others (specifically from $\frac{c_p}{R_g}$ and $\frac{p_{out}}{p_{in}}$), given their bijective relations with these. The obtained dimensionless parameters are summarized in table 1.

Table 1. List of the dimensionless parameters derived via the dimensional analysis of the expander and used for the estimation of its power and isentropic efficiency.

Name	Label	Expression
Dimensionless Power	$\hat{P}$	$\frac{P}{\sqrt{R_g T_{in}} p_{in} r_{ext}^2}$
Isentropic Efficiency	η_{is}	-
Heat Capacity Ratio	γ	$\frac{c_p}{c_v}$
Dimensionless Viscosity	$\hat{\mu}$	$\frac{\mu\sqrt{R_g T_{in}}}{p_{in} r_{ext}}$
Expansion Ratio	β_{exp}	$\frac{p_{in}}{p_{out}}$
Dimensionless Inlet Port Diameter	$\hat{D}_{in}$	$\frac{D_{in}}{r_{ext}}$
Ratio of Radii	$\hat{r}$	$\frac{r_{in}}{r_{ext}}$
Dimensionless Vane Length	$\hat{L}$	$\frac{L}{r_{ext}}$
Dimensionless Vane Thickness	$\hat{b}$	$\frac{b}{r_{ext}}$
Number of Vanes	z	-
Inlet Port Angle	θ_{in}	-
Exhaust Port Opening Angle	θ_{out}	-
Dimensionless Rotational Speed	$\hat{N}$	$\frac{N r_{ext}}{\sqrt{R_g T_{in}}}$

As a result, the dimensionless problem is represented by Equations 4 and 5, and when all the dimensionless variables in brackets have the same values, the machine is operated in similitude conditions and should have the same $\hat{P}$ and η_{is}. Finally, in the present study only geometrically similar machines are considered and their application is constrained to air and hydrogen as working fluids. Consequently, the dimensionless parameters that influence the problem are reduced to the expansion ratio β_{exp}, the dimensionless viscosity $\hat{\mu}$ and the dimensionless rotational speed $\hat{N}$.

3 Experimental validation of the analysis

The goal of the experimental campaign is the construction of two dimensionless performance maps. The experimental campaign is conducted on the 15M1600R-D6 air rotary vane expander manufactured by FIAM. The test bench is described by the diagram in Figure 1 also including all the instrumentation installed. It includes thermocouples (TT-1 and TT-2) and pressure transmitters (PT-1 and PT-2) at the inlet and at the outlet of the machine. A thermal mass flow meter is placed upstream of the expander (ΔTT-1). Pressures are controlled manually thanks to the upstream pressure regulator

(PR-1) and the downstream valve (NV-1). The rotational speed is controlled by varying the excitation voltage of the electric generator (GE-1) coupled with the expander. The voltage is imposed by a DC power supply (DC-1) while the generator is connected to an passive DC load (RE-1) through a diode bridge (BR-1). Measurements of the rotational speed are with a fixed tachometer (TM-1) made by a photodiode. The complete test bench is shown in Figure 2. Finally, the test bench is coupled with a dilution system, ensuring to vent a non-flammable mixture even when operataing with hydrogen [12]. The main parameters of the measuring systems are summarized in table 2. Data acquisition is managed by a custom-built program developed in LabVIEW.

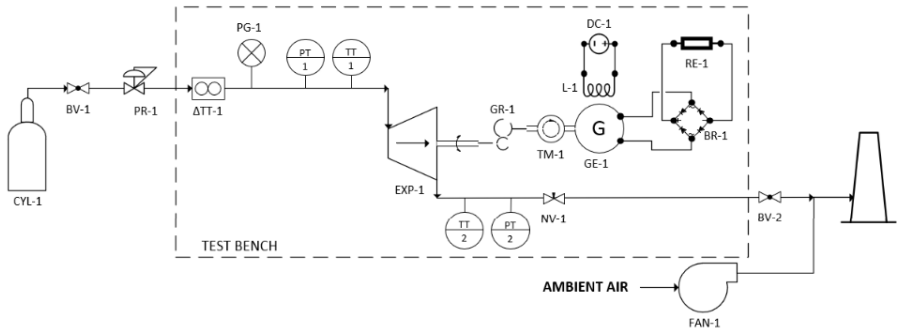


Fig. 1. Process and instrumentation diagram of the experimental apparatus, including all the components of the system, the gas distribution lines of the laboratory facility, and the dilution system for venting hydrogen.

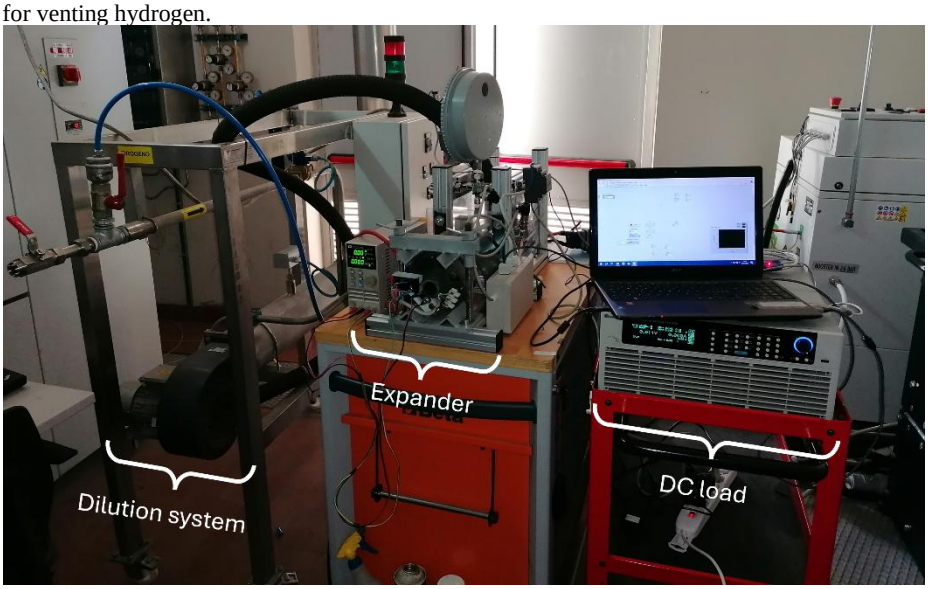


Fig. 2. Experimental apparatus including the test bench, the electronic load, and the dilution system for venting hydrogen.

Table 2. Instrumentation installed in the experimental apparatus and exploited for the validation of the dimensional analysis of the rotary vane expander. Fs stands for "full-scale", Rd stands for "Read value". Volumes refer to normal conditions (273.15 K and 101.325 kPa).

Measure	Instrument	Range	Uncertainty
Gas flow rate	Bronkhorst F113-AI	0-30 m^3/h	±0.1%Fs ±0.5%Rd
Temperature	Calibrated K-type thermocouple	-200-1100°C	±0.05 °C
Pressure	GEMS-3100 series	0-10 bar(a)	±0.25%Fs

4 Results and discussion

The experimental campaign allows for the construction of a series of performance maps at different expansion ratios. Tests aimed at the construction of the performance map are conducted with air at inlet pressures ranging from 2.69 to 6.29 bar(g) and expansion ratios of 2.0, 2.5, and 3.0. Expansion ratios were chosen to maximize the range of inlet pressures. Similarity in heat capacity ratio (γ) enables the comparison of the working conditions between air and hydrogen cases. However, a much higher value of R_g of hydrogen with respect to that of air, imposes that similitude conditions for the dimensionless viscosity $\hat{\mu}$ can be met only by increasing the inlet pressure of hydrogen. These conditions cannot be reached due to the technical limitations of the hydrogen venting system. Nevertheless, tests with hydrogen are performed to extend the domain of the performance map, obtained with air, to higher values of $\hat{\mu}$ and validate the quality of the performance estimations. As a result, the data collected with hydrogen with an inlet pressure of 3.49 bar(g) and with an expansion ratio of 2.5 are used to extend the domain of the middle layer to a maximum $\hat{\mu}$ of $1.2 \cdot 10^{-6}$ for such an expansion rate. The set of data obtained is summarized in table 3.

Table 3. Set of measurements carried out for the construction of the maps of dimensionless power and of isentropic efficiency by varying the working fluid and the inlet pressure

Gas	p_{in} [bar(g)]	p_{out} [bar(g)]	Expansion ratio	Power output [W]
Air	From 2.69±0.03 to 6.29±0.03	From 0.83±0.03 to 2.64±0.03	2	From 14.9±0.3 to 40.2±0.5
Air	From 2.99±0.03 to 6.29±0.03	From 0.59±0.03 to 1.91±0.03	2.5	From 13.1±0.3 to 56.8±0.6
Air	From 3.99±0.03 to 6.29±0.03	From 0.65±0.03 to 1.42±0.03	3	From 23.1±0.4 to 72.1±0.7
H_2	3.49±0.03	0.79±0.03	2.5	From 47.8±0.7 to 91.0±1.0

After performing the measurements, the dimensionless parameters are calculated as defined in section 2 and reported in a dimensionless power map in Figure 3. The map quantifies the dimensionless power as a function of the dimensionless rotational speed ($\hat{N}$) and viscosity ($\hat{\mu}$).

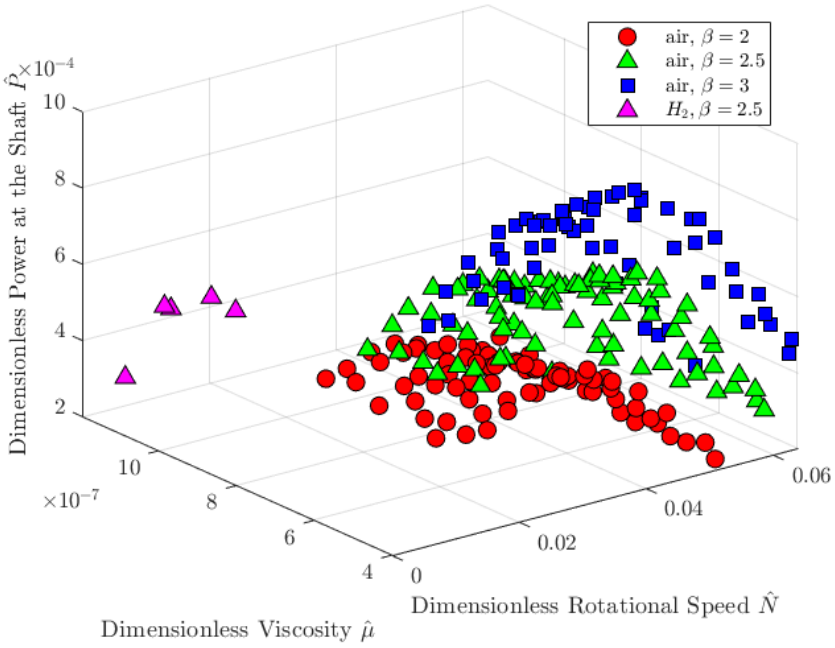


Fig. 3. Air and hydrogen experimental points for the dimensionless power $\hat{P}$, in $\hat{N} - \hat{\mu}$-domain.

The evaluation of performances in similitude conditions is performed through the fitting of the experimental data. The model used for data fitting is polynomial in the form:

$$\hat{P} = p_{00} + p_{10}\hat{N} + p_{01}\hat{\mu} + p_{11}\hat{N}\hat{\mu} + p_{20}\hat{N}^2 \tag{4}$$

A minimum value of 0.9323 was encountered for R^2 and the root mean square error never exceeded 10% of the value of $\hat{P}$ or η_{is} of an experimental point.

As it can be observed in Figure 4, the trend of $\hat{P}$ with respect to $\hat{N}$ is parabolic. An increase in the dimensionless viscosity $\hat{\mu}$ leads to an approximately linear decrease (that becomes more pronounced for higher expansion ratios) in $\hat{P}$. The same trends are observed on the $\hat{N}$-$\hat{\mu}$-η_{is} performance map. The dimensionless viscosity $\hat{\mu}$ reflects the influence of dynamic viscosity and inlet pressure. Increasing the inlet pressure decreases $\hat{\mu}$, corresponding to a rise in shaft power. This is likely related to the improvement of chamber filling during intake as a consequence of the higher inlet pressure. As a result, the volumetric efficiency and the output power are enhanced. Conversely, when dynamic viscosity increases due to a change in fluid, the output power decreases

because higher viscosity causes greater viscous losses. Additionally, it must be noted that the dimensionless viscosity is closely related to the inverse of the Reynolds number. Since a linear relationship between this parameter and the loss of power is evidenced by the experimental data, this indicates a laminar flow regime in the region where viscous losses take place [13]. Among the fitting coefficients, the one that shows the widest confidence interval is p_{11}, related to the product between the dimensionless viscosity and the dimensionless rotational speed. This suggests that the product may have little significance for the analysis. This consideration is further supported by the fact that the effects associated with the Mach and Reynolds numbers, to which the two parameters are closely related, are generally separable [14].

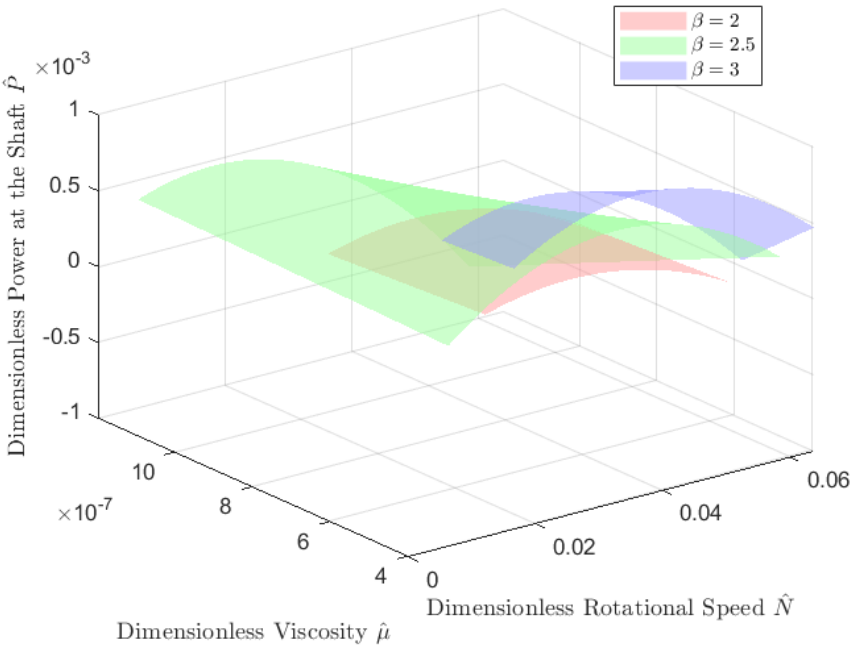


Fig. 4. Surfaces of the performance map obtained by fitting the experimental data. The layer related to an expansion ratio of 2.5 is obtained by fitting data of both hydrogen and air.

The maps obtained can be used for the estimation of the performances in similitude conditions according to the dimensional analysis. Such an estimation is validated with a dedicated set of experimental measurements. These measurements are carried out both with hydrogen and air. The results are reported in Table 4 and Table 5, and can be visualized in Figure 5. Measures with hydrogen are used for the evaluation of the accuracy of the estimation at constant expansion ratio. Indeed, tests conducted with hydrogen with an inlet pressure of 4.49 bar(g) and expansion ratio of 2.5 are used to evaluate the capability of the model in calculating the performances. The results of these tests are represented by the red crosses in Figure 5. The performance of the expander

for expansion ratios between those of the layers of the maps is estimated by linear interpolation of the fitting coefficients of the curves. The effectiveness of this method is validated through a series of tests conducted with air.

The accuracy of the calculation of performances operating with hydrogen shows a maximum error of 3.51% for the dimensionless power and 6.74% for the isentropic efficiency. These results suggest that the proposed method can effectively predict the performance of the rotary vane expander with gases that show similar values of heat capacity ratio. Linear interpolation of the fitting coefficients showed to be an accurate method to estimate the performance of the machine for expansion ratios that were not studied extensively, since the maximum registered error is 4.80% for the dimensionless power and 4.58% for the isentropic efficiency. All these results are reported with greater detail in Table 5 considering both dimensionless power and isentropic efficiency.

The inclusion of the heat capacity ratio γ among the dimensionless parameters influencing the performances prevents the direct application of the performance map previously illustrated with fluids as argon and carbon dioxide. However, a reformulation of the problem based on dimensional variables could be considered, incorporating the volumetric expansion ratio. It could serve as a new dimensionless parameter of significance for the analysis. Preliminary tests with such fluids have already been executed and will be the basis of future investigations into this topic.

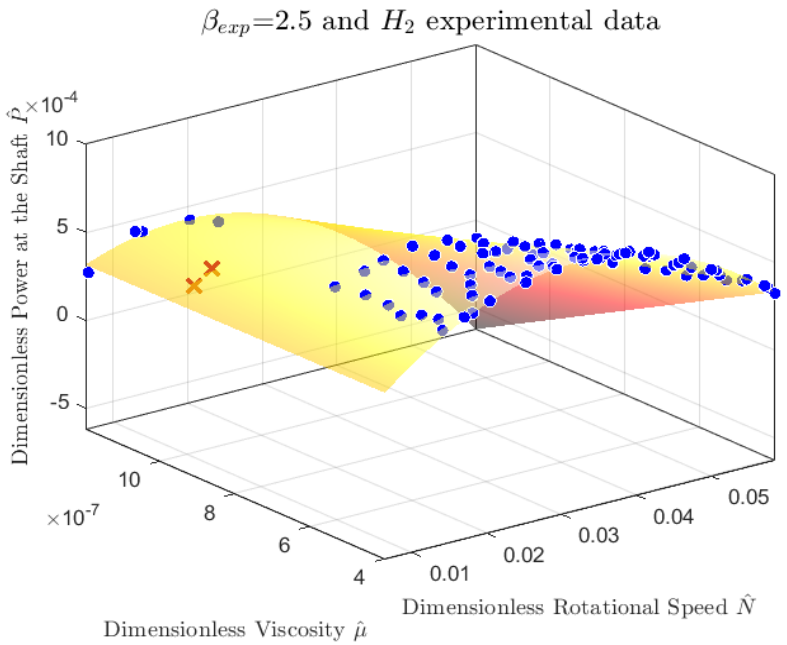


Fig. 5. Validation points collected using hydrogen (marked with a cross) on the surface associated with β_{exp}=2.5 of the performance map.

Table 4. Measured operational conditions of tests for the validation of the performance maps

Gas	T_{in} [°C]	T_{out} [°C]	p_{in} [bar(g)]	p_{out} [bar(g)]	$\dot{V}$ [SL/h]	N [rpm]
H_2	25.88±0.05	19.24±0.05	4.52±0.03	1.20±0.03	32890±90	5480±40
H_2	25.87±0.05	18.36±0.05	4.49±0.03	1.18±0.03	33900±90	7010±50
Air	19.10±0.05	7.04±0.05	5.99±0.03	1.44±0.03	15290±50	5260±20
Air	19.21±0.05	7.79±0.05	5.04±0.03	1.19±0.03	13060±40	5210±30
Air	13.53±0.05	5.01±0.05	4.06±0.03	1.19±0.03	11130±40	5000±30
Air	13.72±0.05	3.71±0.05	4.06±0.03	0.84±0.03	11140±40	4560±50

Table 5. Validation of the performance maps with air and hydrogen evaluating the dimensionless power and the isentropic efficiency

Gas	β_{exp}	$\widehat{P}_{pred} \cdot 10^{-4}$	$\widehat{P} \cdot 10^{-4}$	$\widehat{P}$-error	$\eta_{is,pred}$ (%)	η_{is} (%)	η_{is}-error
H_2	2.51±0.04	3.84	3.71±0.06	3.51%	10.2	9.5±0.4	6.74%
H_2	2.51±0.04	4.27	4.35±0.07	2.03%	10.6	10.7±0.4	0.88%
Air	2.87±0.04	9.20	9.46±0.06	2.74%	15.5	15.7±0.4	1.80%
Air	2.76±0.05	8.25	8.84±0.07	6.70%	14.7	15.4±0.5	4.58%
Air	2.37±0.05	6.33	6.65±0.08	4.80%	13.4	13.4±0.4	0.73%
Air	2.75±0.06	7.67	7.80±0.09	1.67%	14.2	13.7±0.5	3.30%

The results presented are all obtained with the same rotary vane expander. Moreover, the flow regime in the ducts inside the expander is likely laminar, as the linear relationship between the dimensionless viscosity and the loss of power is present in the experimental data. Therefore, this linearity between the dimensionless viscosity and power is expected not to be respected if the geometry of the ducts is varied leading to turbulent conditions. Ultimately, a shortcoming of the current investigation is the lack of a validation of the dimensional analysis when varying the geometrical parameters of the expander. Such a shortcoming is addressed with further tests on a larger rotary vane expander with a test rig under construction.

5 Conclusions

This work developes an effective method to characterize rotary vane expanders using the dimensional analysis, which is validated with an experimental campaign performed with both air and hydrogen while also varying the feed pressure to the expander itself. The main conclusions are summarized as follows.

- The performance parameters of the rotary vane expander in the proposed dimensionless model, namely the dimensionless power $\hat{P}$ and isentropic efficiency η_{is}, can be expressed as a function of three parameters for geometrically similar machines and fluid with a similar heat capacity ratio γ: the expansion ratio β_{exp}, the dimensionless rotational speed $\widehat{N}$ and the dimensionless viscosity $\hat{\mu}$.
- The model is validated showing a good accuracy in making predictions of the performance with compressed hydrogen, leaving a maximum error of 3.51% for the dimensionless power and 6.74% for the isentropic efficiency.

- The dimensionless power and the isentropic efficiency can be accurately predicted for expansion ratios included in the range of those tested for the construction of the maps by means of linear interpolation, showing a maximum error of 4.80% for the dimensionless power and 4.58% for the isentropic efficiency.

In short, the model created in this work is useful for the design and optimization of a rotary vane expander tailored for compressed hydrogen applications. Therefore, it is possible to test a rotary vane expander with air and predict its performance with hydrogen at higher pressures, reducing costs and avoiding the need for special high-pressure equipment.

Nomenclature

N_s	Specific Rotational Speed [-]
D_s	Specific Diameter [-]
P	Power [W]
η_{is}	Isentropic Efficiency [-]
T_{in}	Inlet Temperature [K]
p_{in}	Inlet Pressure [Pa]
p_{out}	Outlet Pressure [Pa]
c_p	Specific Heat at Constant Pressure [J/(kg·K)]
R_g	Gas Constant per Unit of Mass [J/(kg·K)]
μ	Dynamic Viscosity [Pa·s]
D_{in}	Inlet Port Diameter [m]
r_{in}	Internal Radius of the Expander [m]
r_{ext}	External Radius of the Expander [m]
L	Length of the Vane [m]
b	Vane Thickness [m]
θ_{in}	Inlet Port Angle [-]
θ_{out}	Outlet Port Opening Angle [-]
z	Number of Vanes [-]
N	Rotational Speed [s^{-1}]
γ	Heat Capacity Ratio [-]
M	Mach Number [-]

For the other dimensionless parameters, refer to Table 1.

References

1. Staffel I, Dodds P, Scamman D, et al. The Role of Hydrogen Energy. *Hydrog Econ*. 2017;(March):1-33. doi:10.1016/b978-0-12-811132-1.00001-8
2. British Standard. ISO 2787:1984, BS 5344:1985 Methods for performance tests for rotary and percussive pneumatic tools. Published online 1985.
3. Badr O, O'Callaghan PW, Probert SD. Multi-vane expanders: Geometry and vane kinematics. *Appl Energy*. 1985;19(3):159-182. doi:10.1016/0306-

2619(85)90006-6
4. Badr O, Probert SD, O'Callaghan PW. Multi-vane expanders: Internal-leakage losses. *Appl Energy*. 1985;20(1):1-46. doi:10.1016/0306-2619(85)90033-9
5. Badr O, O'Callaghan PW, Probert SD. Multi-vane expander performance: Breathing characteristics. *Appl Energy*. 1985;19(4):241-271. doi:10.1016/0306-2619(85)90001-7
6. Longo S. *Analisi Dimensionale e Modellistica Fisica: Principi e Applicazioni Alle Scienze Ingegneristiche*. Springer Milan; 2011.
7. Narasimhan AK, Wickramaratne C, Kamal R, Goswami DY, Singh P. Mapping scroll expander performance for organic working fluids using dimensionless parameters in Ns-Ds diagram. *Energy*. 2019;182:739-752. doi:10.1016/j.energy.2019.06.054
8. Olmedo LE, Mounier V, Mendoza LC, Schiffmann J. Dimensionless correlations and performance maps of scroll expanders for micro-scale Organic Rankine Cycles. *Energy*. 2018;156:520-533. doi:10.1016/j.energy.2018.05.001
9. Francesconi M, Dori E, Antonelli M. Analysis of Balje diagrams for a Wankel expander prototype. *Appl Energy*. 2019;238(December 2018):775-785. doi:10.1016/j.apenergy.2019.01.096
10. Buckingham E. On physically similar systems; Illustrations of the use of dimensional equations. *Phys Rev*. 1914;4(4):345-376. doi:10.1103/PhysRev.4.345
11. Badr O, Probert SD, O'Callaghan P. Multi-vane expanders: Vane dynamics and friction losses. *Appl Energy*. 1985;20(4):253-285. doi:10.1016/0306-2619(85)90018-2
12. Battistella F, Ravidà A, Mastromatteo M, Pinna RS, Valenti G. Development of an experimental apparatus and a data analysis protocol for the test of hydrogen volume and flow meters in controlled environmental conditions. *E3S Web Conf*. 2021;312. doi:10.1051/e3sconf/202131204001
13. Das GP. *Hydraulic Engineering: Fundamental Concepts*. Momentum Press; 2016.
14. Modesti D, Pirozzoli S. Reynolds and Mach number effects in compressible turbulent channel flow. *Int J Heat Fluid Flow*. 2016;59:33-49. doi:10.1016/j.ijheatfluidflow.2016.01.007